Article
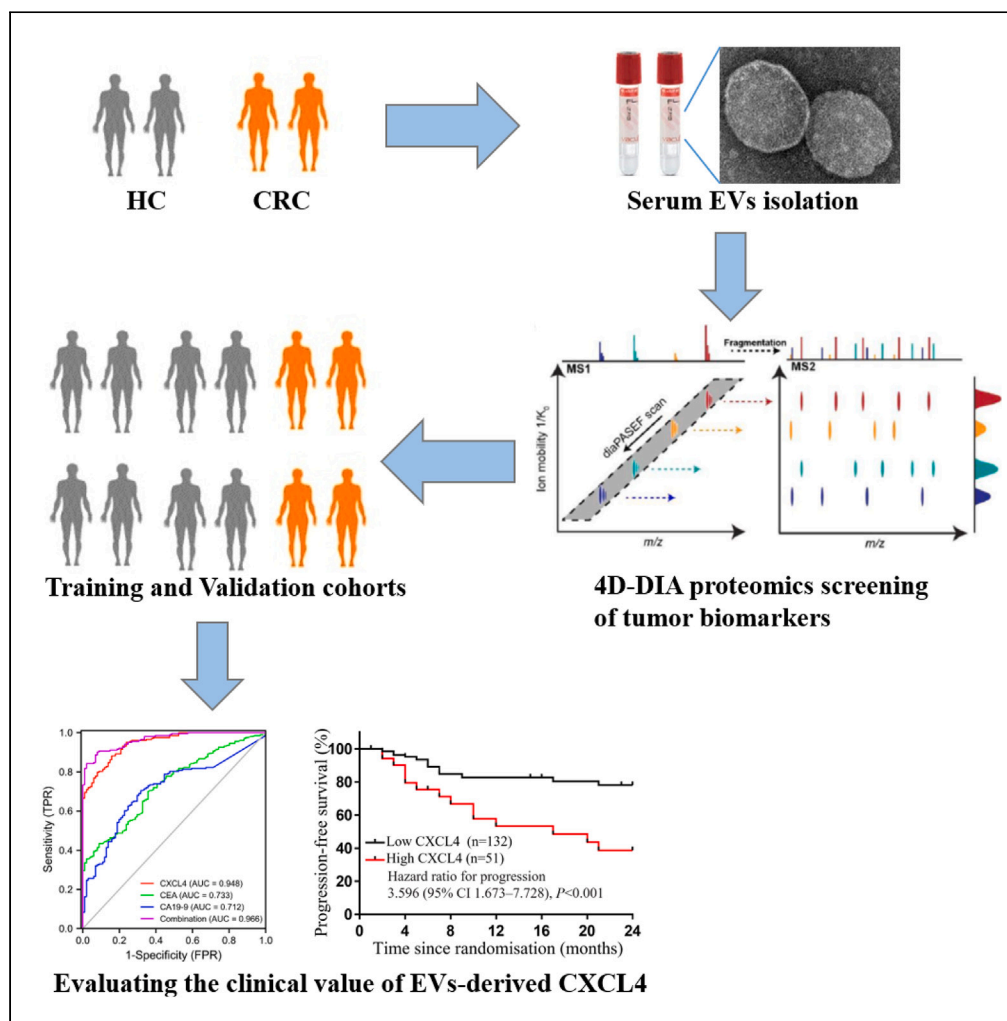
Extracellular vesicles-derived CXCL4 is a candidate serum tumor biomarker for colorectal cancer

Jinye Xie, Shan Xing, Hongbo Jiang, ..., Shiqiong Niu, Zhijian Huang, Haofan Yin

120354833@qq.com (S.N.)
huangzhj29@mail2.sysu.edu.cn (Z.H.)
yinhf@mail2.sysu.edu.cn (H.Y.)

Highlights

Proteomics identified CXCL4 elevated in serum EVs of CRC patients

Serum EVs-derived CXCL4 emerged as a diagnostic and prognostic biomarker for CRC

Article

Extracellular vesicles-derived CXCL4 is a candidate serum tumor biomarker for colorectal cancer

Jinye Xie,[1,9] Shan Xing,[5,6,9] Hongbo Jiang,[3,9] Jiaju Zhang,[7] Daxiao Li,[8] Shiqiong Niu,[3,*] Zhijian Huang,[4,*] and Haofan Yin[2,3,10,*]

SUMMARY

Extracellular vesicles (EVs) were promising circulating biomarkers for multiple diseases, but whether serum EVs-derived proteins could be used as a reliable tumor biomarker for colorectal cancer (CRC) remained inconclusive. In this study, we identified CXCL4 by a 4D data-independent acquisition-based quantitative proteomics assay of serum EVs-derived proteins in 40 individuals and subsequently analyzed serum EVs-derived CXCL4 levels by ELISA in 2 cohorts of 749 individuals. The results revealed that EVs-derived CXCL4 levels were dramatically elevated in CRC patients than in benign colorectal polyp patients or healthy controls (HC). Furthermore, receiver operating characteristic curves revealed that EVs-derived CXCL4 exhibited superior diagnostic performance with area under the curve of 0.948 in the training cohort. Additionally, CXCL4 could effectively distinguish CRC in stage I/II from HC. Notably, CRC patients with high levels of EVs-derived CXCL4 have shorter 2-year progression-free survival than those with low levels. Overall, our findings demonstrated that serum EVs-derived CXCL4 was a candidate diagnostic and prognostic biomarker for CRC.

INTRODUCTION

The incidence and progression of colorectal cancer (CRC) were influenced by numerous factors, including genetic mutations, unhealthy lifestyles, and gut microbiota dysbiosis.[1,2] Estimates suggest that the 5-year relative survival rate of CRC patients decreased sharply from 90% in the early stage to 20% in the progression stage, emphasizing the importance of early diagnosis to reduce mortality.[3] The evolution from precursor lesions to cancer took approximately 10 years, which provided a long window of time for prevention and early diagnosis of CRC.[4] Endoscopy remained the gold standard for diagnosing CRC, but limited medical resources prevented it from being a mass screening method.[5] In terms of noninvasive detection methods, two of the most commonly used biomarkers for CRC diagnosis are CEA and CA19-9.[6] However, several studies have proven that CEA and CA19-9 lacked sufficient sensitivity and were more suitable for dynamic monitoring of CRC patients during treatment.[7,8] As a result, it was essential to explore candidate tumor biomarkers for the noninvasive detection of CRC.

Extracellular vesicles (EVs) were vectors for cellular communication, carrying a rich cargo of nucleic acids and proteins, which could be transported between cells to drive specific biological functions.[9] Recent evidence has suggested that non-coding RNAs carried by EVs isolated from body fluids such as plasma, urine, and saliva had the potential capacity to act as tumor biomarkers.[10] For instance, miR-139-3p, miR-145-3p, miR-150-3p, and let-7b-3p have been identified as biomarkers of CRC in plasma EVs.[11] Advances in droplet digital PCR technology had enabled further investigations into the diagnostic potential of non-coding RNAs packaged in EVs; however, progress in understanding the protein content of EVs derived from blood had been hindered by the limitations of past proteomics approaches. Actually, EVs proteins were more stable than non-coding RNAs during prolonged storage, which was essential for applications in clinical testing.[12] Therefore, the

[1]Department of Laboratory Medicine, Zhongshan City People's Hospital, Zhongshan, Guangdong, China
[2]Department of Laboratory Medicine, Shenzhen People's Hospital (The Second Clinical Medical College, Jinan University, The First Affiliated Hospital, Southern University of Science and Technology), Shenzhen, Guangdong, China
[3]Department of Clinical Laboratory, The Seventh Affiliated Hospital of Sun Yat-sen University, Shenzhen, Guangdong, China
[4]Department of Pathology, The Seventh Affiliated Hospital of Sun Yat-Sen University, Shenzhen, Guangdong, China
[5]Department of Clinical Laboratory, State Key Laboratory of Oncology in South China, Sun Yat-sen University Cancer Center, Guangzhou, Guangdong, China
[6]School of Biomedical Engineering, Sun Yat-sen University, Guangzhou, Guangdong, China
[7]Department of Laboratory Medicine, Zhujiang Hospital, Southern Medical University, Guangzhou, Guangdong, China
[8]Department of Ophtalmology and ENT, Shenzhen Longgang District Second People's Hospital, Shenzhen, Guangdong, China
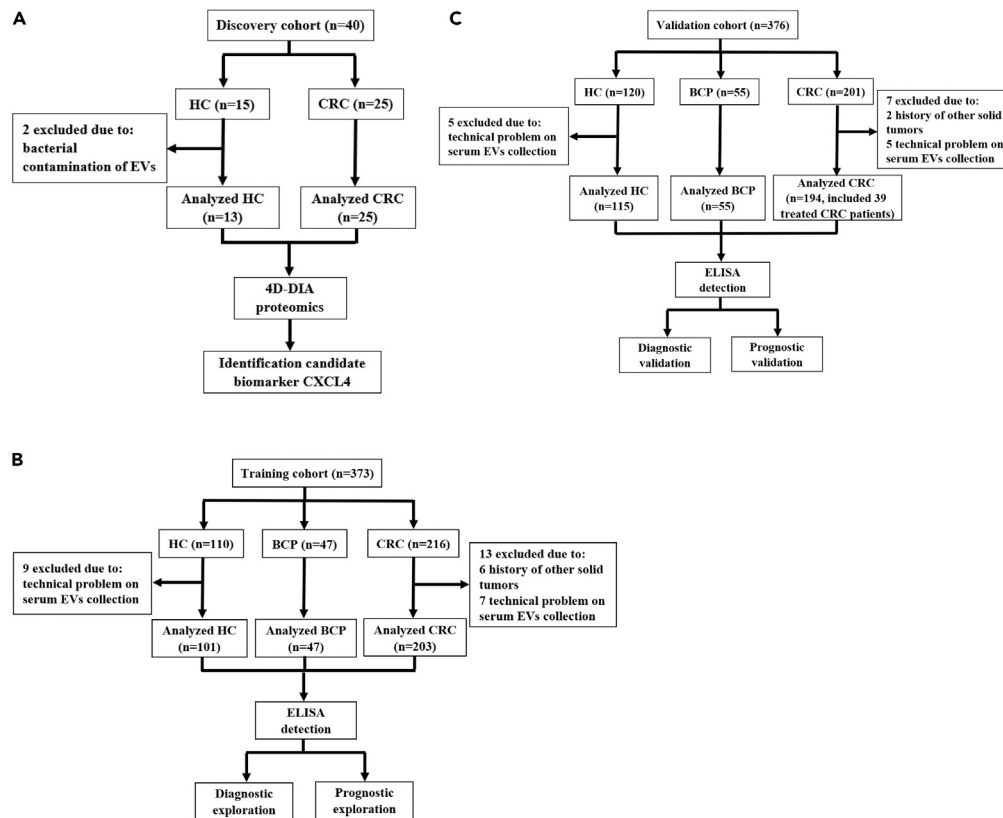[9]These authors contributed equally
[10]Lead contact
*Correspondence: 120354833@qq.com (S.N.), huangzhj29@mail2.sysu.edu.cn (Z.H.), yinhf@mail2.sysu.edu.cn (H.Y.)
https://doi.org/10.1016/j.isci.2024.109612

Figure 1. Clinical study design flowchart and workflow

(A–C) Clinical study design flowchart depicting the recruitment from the discovery cohort (A), training cohort (B), and validation cohort (C).

application of the latest proteomics technologies to explore the protein components of serum-derived EVs has the potential to uncover more promising tumor biomarkers.

CXCL4 (chemokine C-X-C motif ligand 4) had been found to exert both antitumor effects by inhibiting angiogenesis and pro-tumor effects by modulating the immune microenvironment.[13–15] It was generally believed that CXCL4 was mainly stored in tumor cells and platelets.[16] Additionally, recent studies have successively identified roles for CXCL4 in diverse non-neoplastic diseases, such as serving as a biomarker of systemic sclerosis and a restrictor for respiratory syncytial virus infection correlated with the severity of clinical symptoms in patients.[17,18] Besides, CXCL4 associated with the induction of fibroblast differentiation and collagen synthesis, which promoted fibrosis.[19,20] Our previous investigation indicated that tumor-associated macrophages secreting CXCL1 and CXCL5, family members of CXCL4, activated the CXCR2/STAT3 positive feedback pathway in gastric cancer cells and promoted tumor metastasis.[21,22] Yet, the role of CXCL4 in gastrointestinal tumors remains largely unexplored, particularly with regard to its role in EVs-derived CXCL4 in the diagnosis and prediction of CRC.

In the present study, we aimed to use 4D data-independent acquisition (4D-DIA) proteomics to deeply analyze the expression profile of serum EVs proteins in CRC patients and identified EVs-derived CXCL4 as a candidate tumor biomarker. ELISA was then applied to measure the levels of serum EVs-derived CXCL4 in two cohorts of 749 individuals in order to assess its diagnostic and prognostic role in CRC. Besides, our results revealed that serum-free CXCL4 failed to serve as a reliable tumor biomarker for CRC, in contrast to serum EVs-derived CXCL4.

RESULTS

Identification of enriched proteins in serum EVs of CRC patients by 4D-DIA proteomics

A total of 789 individuals were recruited, comprising 40 in the discovery cohort, 373 in the training cohort, and 376 in the validation cohort (Figures 1A–1C). The workflow for identifying serum EVs-derived protein as a candidate biomarker for CRC was displayed in Figure 1D. For the discovery cohort of 25 CRC patients and 13 healthy controls (HC), isolated EVs from serum were confirmed by western blot, nanoparticle tracking analysis (NTA), and transmission electron microscopy (TEM) (Figures 2A–2C). Western blot analysis exposed CD63 and TSG101 expression in isolated EVs but not in peripheral blood mononuclear cell (Figure 2A). Intracellularly enriched proteins grp94 and calnexin, used as negative control biomarkers for EVs recognition, were not detected in our isolated EVs (Figure 2A). Besides, the size and number of EVs samples were analyzed by NTA in 10 randomly selected cases from each of the HC, benign colorectal polyp (BCP), and CRC groups in the training cohort (Figure 2B). While there were no discernible differences in the size distribution of EVs among these three groups, a
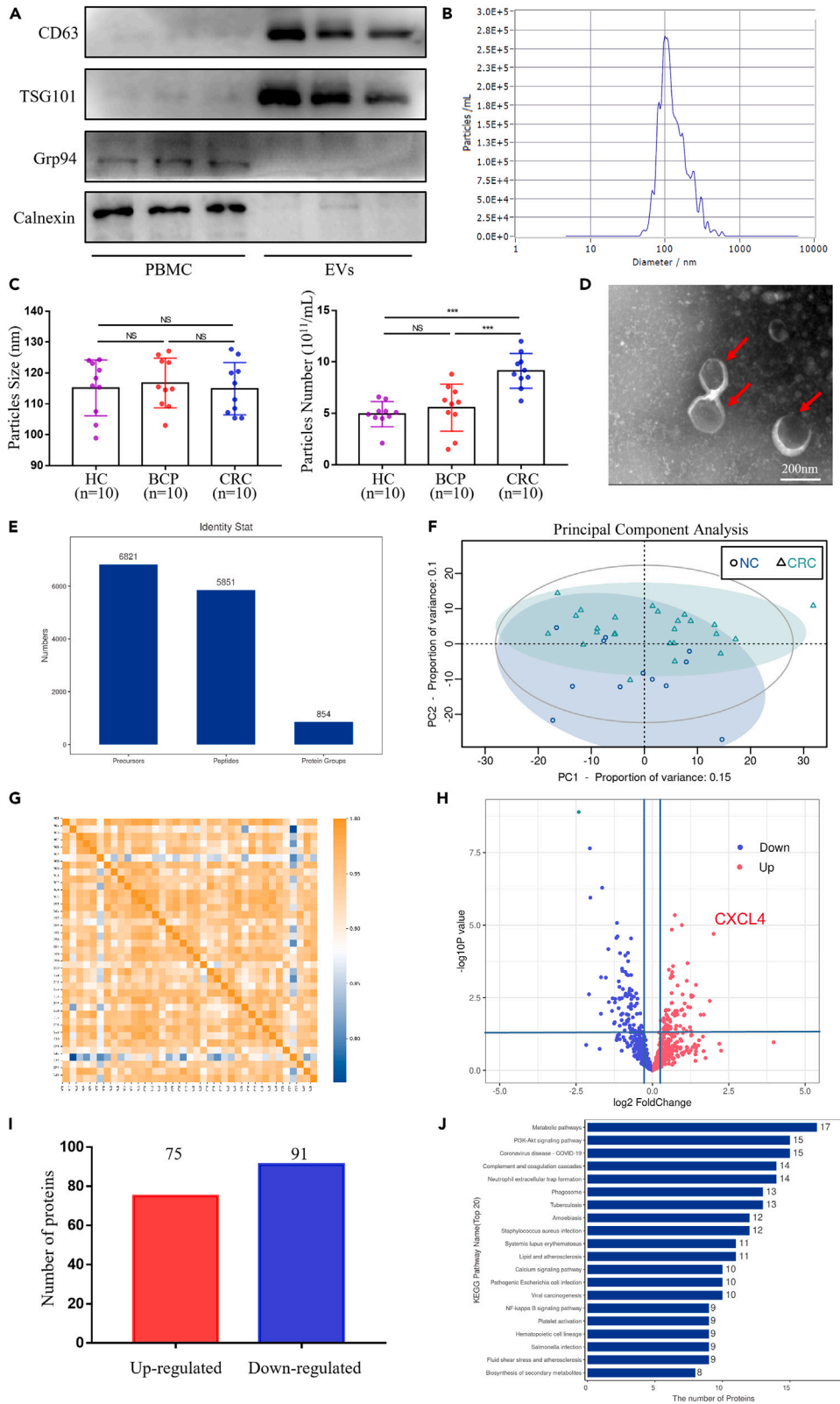
Figure 2. Identification of enriched proteins in serum EVs of CRC patients by 4D-DIA proteomics

(A) Western blot analysis of EVs markers CD63 and TSG101 in isolated serum EVs of CRC. Grp94 and Calnexin were used as negative controls.

(B) NTA presented the sizes and distribution of isolated EVs via Flow NanoAnalyzer.

(C) Particle size and number of serum EVs fraction from HC, BCP, and CRC by NTA.

(D) Representative TEM image of EVs isolated from serum. Scale bar, 200 nm.

(E) Number of peptides and proteins in serum EVs from CRC and HC identified by 4D-DIA proteomics.

(F) PCA revealed differences in the proteomics of serum EVs between HC and CRC patients.

(G) PCC of serum EVs proteins in CRC and HC. (H) The volcano plots of DEPs in serum EVs (p < 0.05, fold change >1.2). (I) Number of up-regulated and down-regulated DEPs in serum EVs of CRC.

(J) GO functional analysis of DEPs in serum EVs (biological process, molecular function, and cellular component).

significant increase in the number of EVs was observed in the CRC group compared to both the HC and BCP groups (Figure 2C). TEM further confirmed the presence of round and cup-shaped bilayer membrane vesicle-like structures in serum EVs (Figure 2D). Taken together, these results indicated that EVs isolated from serum samples were satisfactorily collected.

Subsequent in-depth EVs proteome analysis using 4D-DIA technology identified a total of 5,851 peptides and 854 proteins (Figure 2E). Principal component analysis and Pearson's correlation coefficient indicated reproducible intragroup protein quantification and stable inter-group differential proteins (Figures 2F and 2G). Additionally, we revealed 166 differentially expressed proteins (DEPs) in CRC compared with HC, of which 75 were up-regulated and 91 were down-regulated (Figures 2H and 2I). To further characterize the biological function of the DEPs, we performed Gene Ontology (GO) and Kyoto Encyclopedia of Genes and Genomes (KEGG) pathway enrichment analysis. The cellular component of GO analysis revealed DEPs were enriched in the cell part and extracellular region part, while the molecular functions of GO analysis indicated they were associated with catalytic activity (Figure 2J). As for biological processes, DEPs were involved in cellular process and immune system process (Figure 2J). Moreover, KEGG pathway analysis suggested that DEPs were enriched for some pathways involved in cancer, such as metabolic pathways, PI3K-Akt signaling pathway, and platelet activation (Figure S1A). The top 9 up-regulated DEPs and the top 9 down-regulated DEPs were listed in Figures S1B and S1C, among which CXCL4 was found to be the most markedly up-regulated protein in serum EVs of CRC patients.
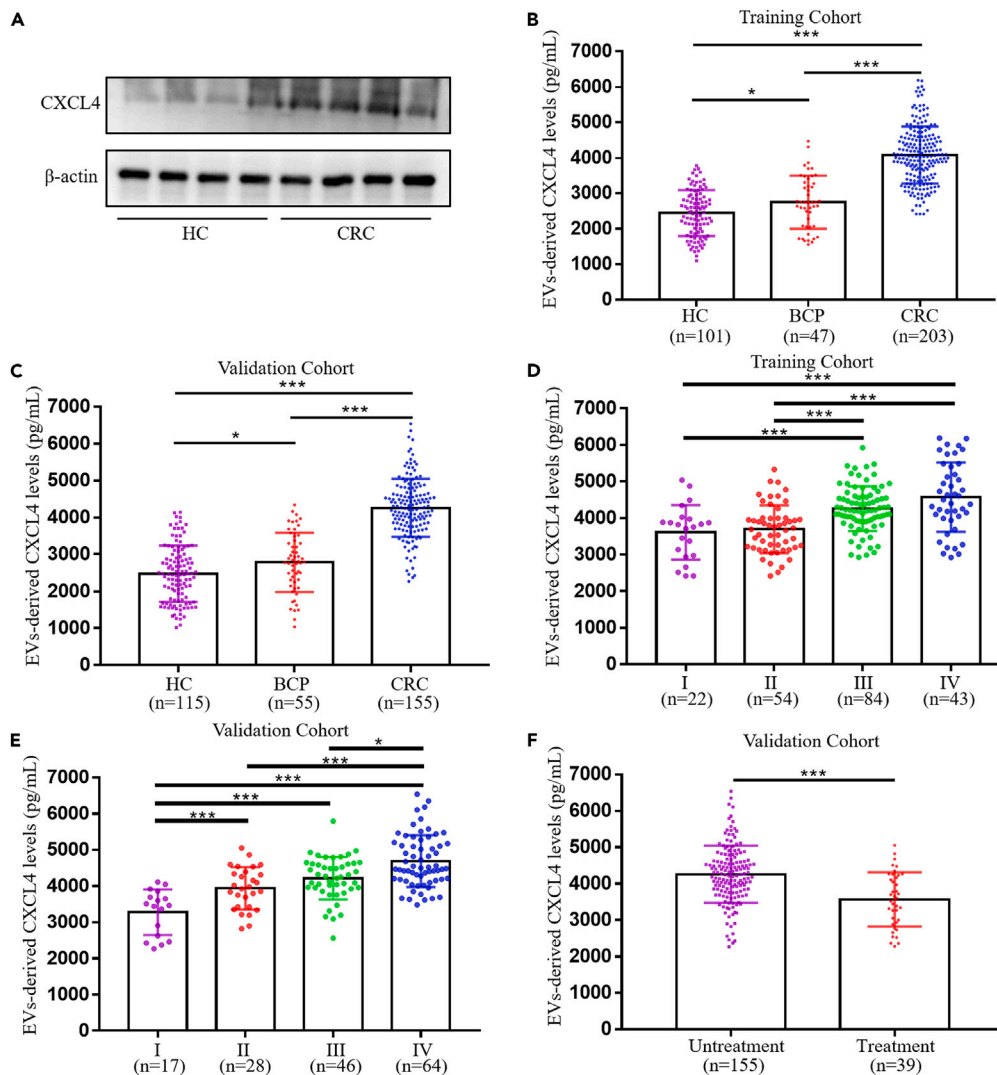
The levels of serum EVs-derived CXCL4 in CRC patients, BCP patients, and HC

Consistent with 4D-DIA proteomics data, western blot results revealed that CXCL4 levels were markedly higher in serum EVs of CRC patients compared to HC (Figure 3A). To further assess the specific levels of serum EVs-derived CXCL4, we extracted serum EVs from 749 participants, including 373 in the training cohort and 376 in the validation cohort, for ELISA detection. The 2 cohorts were well matched for various clinicopathologic characteristics, such as age and gender (Tables S1 and S2). Notably, levels of serum EVs-derived CXCL4 were significantly elevated in both cohorts in CRC patients compared with HC or BCP patients (Figures 3B and 3C). Moreover, the analysis on EVs-derived CXCL4 levels and clinicopathological characteristics of CRC patients suggested its association with clinical stage, TNM classification, and 2-year progression-free survival (PFS) status (Tables S3 and S4). Remarkably, EV-derived CXCL4 level gradually increased as the CRC patient stage progressed in both the training and validation cohorts (Figures 3D and 3E). Interestingly, EV-derived CXCL4 levels were significantly reduced in CRC patients after treatment in the validation cohort (Figure 3F). We further validated our findings in CRC mouse models by collecting serum from a series of CRC mice. Consistent with the results in CRC patients, substantially raised levels of serum EVs-derived CXCL4 were observed in both Apc-L850X mice and MC38 syngeneic mice compared to normal control mice (Figure S2). Collectively, these results point to the potential tumor biomarker roles of serum EVs-derived CXCL4 for CRC.

Diagnostic outcomes for serum EVs-derived CXCL4 in CRC patients

Receiver operating characteristic (ROC) curves were plotted to evaluate the diagnostic efficacy of serum EVs-derived CXCL4. Impressively, EVs-derived CXCL4 in the training cohort exhibited a higher area under the curve (AUC) of 0.948 compared to traditional tumor biomarkers CEA and CA19-9, with AUCs of 0.733 and 0.712, respectively (Figure 4A). Based on the optimal cutoff value (3123.61 pg/mL) of the Youden index obtained from the ROC curve, CRC patients in the training cohort could be discriminated from HC using EVs-derived CXCL4, which resulted in a sensitivity of 88.2% and specificity of 84.2% (Table 1). Meanwhile, the combination of EVs-derived CXCL4, CEA, and CA19-9 slightly increased the AUC to 0.966 (Figure 4A). Furthermore, the validation cohort also confirmed the superior diagnostic performance of EVs-derived CXCL4, with an AUC of 0.946 (Figure 4B). Interestingly, EVs-derived CXCL4 was able to distinguish CRC patients from BCP patients, with an AUC of 0.886 and 0.907 in the training and validation cohorts, respectively (Figures 4C and 4D).

Early-stage tumors were more challenging to diagnose than advanced tumors due to limited biomarker signatures. Thus, we plotted ROC curves to investigate the diagnostic efficacy of serum EVs-derived CXCL4 for early-stage CRC. EVs-derived CXCL4 in the training cohort presented good discrimination ability to identify CRC in stage I and stage II from HC, with AUCs of 0.868 and 0.910, respectively (Figures 4E and 4F; Table S5). Besides, EVs-derived CXCL4 could discriminate early-stage CRC from HC with an AUC of 0.776 for stages I and 0.931 for stage II in the validation cohort (Figures S3A and S3B). As expect, the ability of EVs-derived CXCL4 to identify CRC in stage III and stage IV from HC was further elevated in the training and validation cohort (Figures 4G, 4H, S3C, and S3D). Additionally, EVs-derived CXCL4 was superior to CEA and CA19-9 in distinguishing early-stage CRC from BCP in both cohorts (Figure S4; Table S6). In conclusion, these findings illustrated that serum EVs-derived CXCL4 was a promising diagnostic biomarker for CRC.
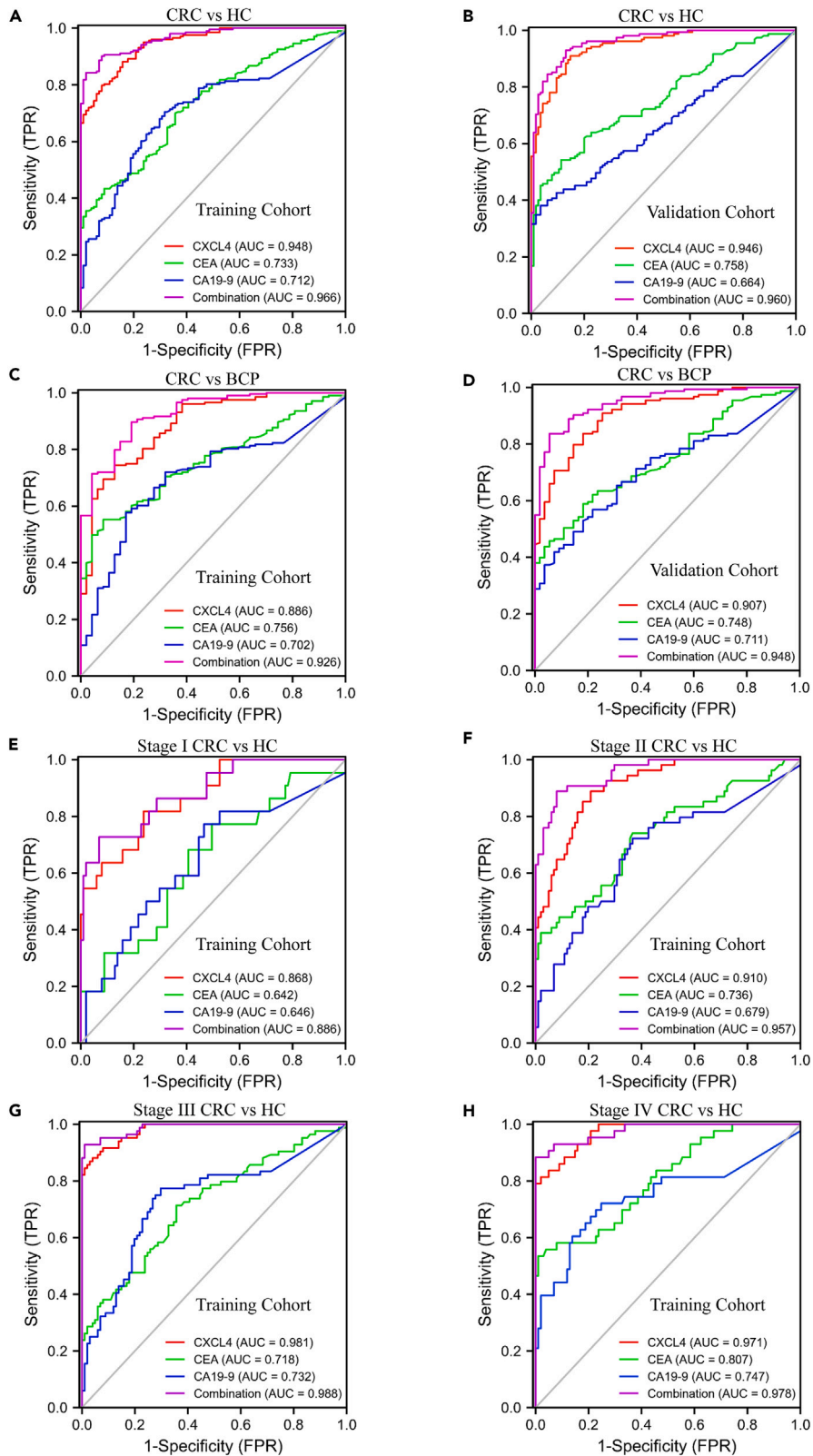
Figure 3. The levels of serum EVs-derived CXCL4 in CRC patients, BCP patients, and HC

(A) Western blot analysis of CXCL4 in serum EVs from HC and CRC patients. β-Actin was used as the internal control.

(B) The levels of serum EVs-derived CXCL4 from CRC patients ($n = 203$), BCP patients ($n = 47$), and HC ($n = 101$) in the training cohort.

(C) The levels of EVs-derived CXCL4 from CRC patients ($n = 155$), BCP patients ($n = 55$), and HC ($n = 115$) in the validation cohort.

(D and E) The levels of EVs-derived CXCL4 at different clinical stages of CRC patients (stage I, $n = 22$; stage II, $n = 54$; stage III, $n = 84$; stage IV, $n = 43$) in the training cohort (D) and CRC patients (stage I, $n = 17$; stage II, $n = 28$; stage III, $n = 46$; stage IV, $n = 64$) in the validation cohort (E).

(F) Comparison of EVs-derived CXCL4 in CRC patients with ($n = 39$) and without ($n = 155$) treatment in the validation cohort. Data are shown as mean ± SD; *p < 0.05, and ***p < 0.001.

Prognostic outcomes for serum EVs-derived CXCL4 in CRC patients

Since serum EVs-derived CXCL4 was strongly associated with 2-year PFS in Tables S3 and S4, we further explored its prognostic role. First, the time-dependent ROC curve analysis was plotted to calculate the AUCs for 1-year and 2-year PFS, which were 0.681 and 0.736, respectively, in the training cohort (Figure 5A). The Youden index obtained from the PFS ROC curve yielded an optimal cutoff value of 4511.79 pg/mL, which was used to divide CRC patients into low and high EVs-derived CXCL4 level groups (Figure 5A). Subsequently, Kaplan-Meier analysis revealed that 2-year PFS was dramatically shorter in CRC patients with high levels of EVs-derived CXCL4 in both the training cohort (hazard ratio [HR] = 3.596, 95% confidence interval [CI] 1.673–7.728) and validation cohort (HR = 2.357, 95% CI 1.171–4.744), suggesting that serum EVs-derived CXCL4 could serve as an indicator of CRC prognosis (Figures 5B and 5C).

Moreover, we conducted univariate Cox regression analysis, which indicated that 2-year PFS was associated with CEA, CA19-9, T classification, N classification, M classification, and EVs-derived CXCL4 in the training cohort (Table 2). Furthermore, the multivariate Cox regression analyses were performed to identify CA19-9, M classification, and EVs-derived CXCL4 that were independent prognostic factors for 2-year

A CRC vs HC — Training Cohort
- CXCL4 (AUC = 0.948)
- CEA (AUC = 0.733)
- CA19-9 (AUC = 0.712)
- Combination (AUC = 0.966)

B CRC vs HC — Validation Cohort
- CXCL4 (AUC = 0.946)
- CEA (AUC = 0.758)
- CA19-9 (AUC = 0.664)
- Combination (AUC = 0.960)

C CRC vs BCP — Training Cohort
- CXCL4 (AUC = 0.886)
- CEA (AUC = 0.756)
- CA19-9 (AUC = 0.702)
- Combination (AUC = 0.926)

D CRC vs BCP — Validation Cohort
- CXCL4 (AUC = 0.907)
- CEA (AUC = 0.748)
- CA19-9 (AUC = 0.711)
- Combination (AUC = 0.948)

E Stage I CRC vs HC — Training Cohort
- CXCL4 (AUC = 0.868)
- CEA (AUC = 0.642)
- CA19-9 (AUC = 0.646)
- Combination (AUC = 0.886)

F Stage II CRC vs HC — Training Cohort
- CXCL4 (AUC = 0.910)
- CEA (AUC = 0.736)
- CA19-9 (AUC = 0.679)
- Combination (AUC = 0.957)

G Stage III CRC vs HC — Training Cohort
- CXCL4 (AUC = 0.981)
- CEA (AUC = 0.718)
- CA19-9 (AUC = 0.732)
- Combination (AUC = 0.988)

H Stage IV CRC vs HC — Training Cohort
- CXCL4 (AUC = 0.971)
- CEA (AUC = 0.807)
- CA19-9 (AUC = 0.747)
- Combination (AUC = 0.978)

Figure 4. Diagnostic outcomes for serum EVs-derived CXCL4 in CRC patients

(A and B) ROC curves to identify CRC from HC with EVs-derived CXCL4, CEA, CA19-9, and the combination of CXCL4 + CEA + CA19-9, respectively, in the training cohort (A) and validation cohort (B).

(C and D) ROC curves to identify CRC from BCP with serum EVs-derived CXCL4 in the training cohort (C) and validation cohort (D).

(E–H) ROC curves to identify CRC in stage I (E), in stage II (F), in stage III (G), and in stage IV (H) from HC with serum EVs-derived CXCL4, respectively, in the training cohort.

PFS (Table 2). To offer more accurate prediction of 2-year PFS in individual CRC patients, we constructed a nomogram prediction model based on multivariate Cox regression analysis (Figure 5D). The calibration plot of the PFS probability at 1 or 2 years after therapy demonstrated agreement between the prediction of the nomogram and actual observation in both cohorts (Figures 5E and S5A). Decision curve analysis further showed a greater net clinical benefit when using the nomogram prediction model that took into account EVs-derived CXCL4, CA19-9, and M classification compared to using only single-risk factors in both the training cohort and validation cohort (Figures 5F, 5G, S5B, and S5C). The nomogram model in the training cohort exhibited a C-index of 0.774 and obtained a C-index of 0.716 in the validation cohort, which far exceeded any individual index, thus demonstrating the model's promising discrimination (Table S7). Taken together, our findings demonstrated that considering various clinical factors enhanced the prediction efficiency of the nomogram model.

The role of serum-free CXCL4 in the diagnosis and prognosis of CRC

Due to the high concentrations of free CXCL4 in serum, we investigated whether serum-free CXCL4 possessed the same diagnostic and predictive role as EVs-derived CXCL4 for CRC. Significantly higher serum-free CXCL4 was found in CRC compared to HC in both cohorts (Figures 6A and 6B). Moreover, a positive correlation existed between serum-free CXCL4 levels and EVs-derived CXCL4 levels in CRC patients (Figures 6C and 6D). However, ROC analysis illustrated that serum-free CXCL4 was less effective than CEA and CA19-9 in distinguishing CRC from HC in both the training cohort and validation cohort (Figures 6E and 6F). According to the optimal cutoff value (61.57 ng/mL) of the Youden index obtained from the 2-year PFS ROC curve in the training cohort, CRC patients were divided into groups with low and high serum CXCL4 levels (Figure S5D). As revealed by Kaplan-Meier analysis, there indicated no clear difference in 2-year PFS in CRC patients with high serum levels of CXCL4 compared to those with low serum levels of CXCL4 in both cohorts (Figures 6G and 6H). Thus, serum-free CXCL4 does not appear to possess the same prospective diagnostic and prognostic value as EVs-derived CXCL4 for CRC.

DISCUSSION

CRC was one of the most common malignant tumors of the digestive system worldwide, with a high incidence and mortality rate.[4] Due to its insidious symptoms in the early stage, more than half of CRC patients were already in an advanced stage at the time of initial diagnosis.[3] Early diagnosis could effectively improve the prognosis of patients, whereas noninvasive diagnostic biomarkers for CRC were lacking in the clinical settings. Our recent research has shown that the RNA methylation modification status of peripheral blood leukocytes could provide superior diagnostic efficacy for CRC.[23,24] Unfortunately, RNA samples were difficult to store, and the process of RNA methylation modification

Table 1. The sensitivity and specificity of various biomarkers tested individually and in combination for the identification of CRC from HC and BCP

Distinction	Cohort	Biomarker	Sensitivity	Specificity	AUC	95% CI
CRC vs. HC	training	CXCL4	0.882	0.842	0.948	0.926–0.970
	training	CEA	0.433	0.911	0.733	0.677–0.789
	training	CA19-9	0.704	0.683	0.712	0.653–0.770
	training	combination	0.842	0.980	0.966	0.949–0.982
	validation	CXCL4	0.910	0.852	0.946	0.921–0.970
	validation	CEA	0.542	0.887	0.758	0.702–0.814
	validation	CA19-9	0.381	0.965	0.664	0.601–0.728
	validation	combination	0.929	0.870	0.960	0.939–0.981
CRC vs. BCP	training	CXCL4	0.744	0.872	0.886	0.834–0.937
	training	CEA	0.552	0.915	0.756	0.693–0.819
	training	CA19-9	0.576	0.830	0.702	0.627–0.777
	training	combination	0.897	0.809	0.926	0.889–0.963
	validation	CXCL4	0.837	0.818	0.907	0.865–0.949
	validation	CEA	0.588	0.818	0.748	0.681–0.815
	validation	CA19-9	0.569	0.782	0.711	0.641–0.781
	validation	combination	0.837	0.945	0.948	0.919–0.977
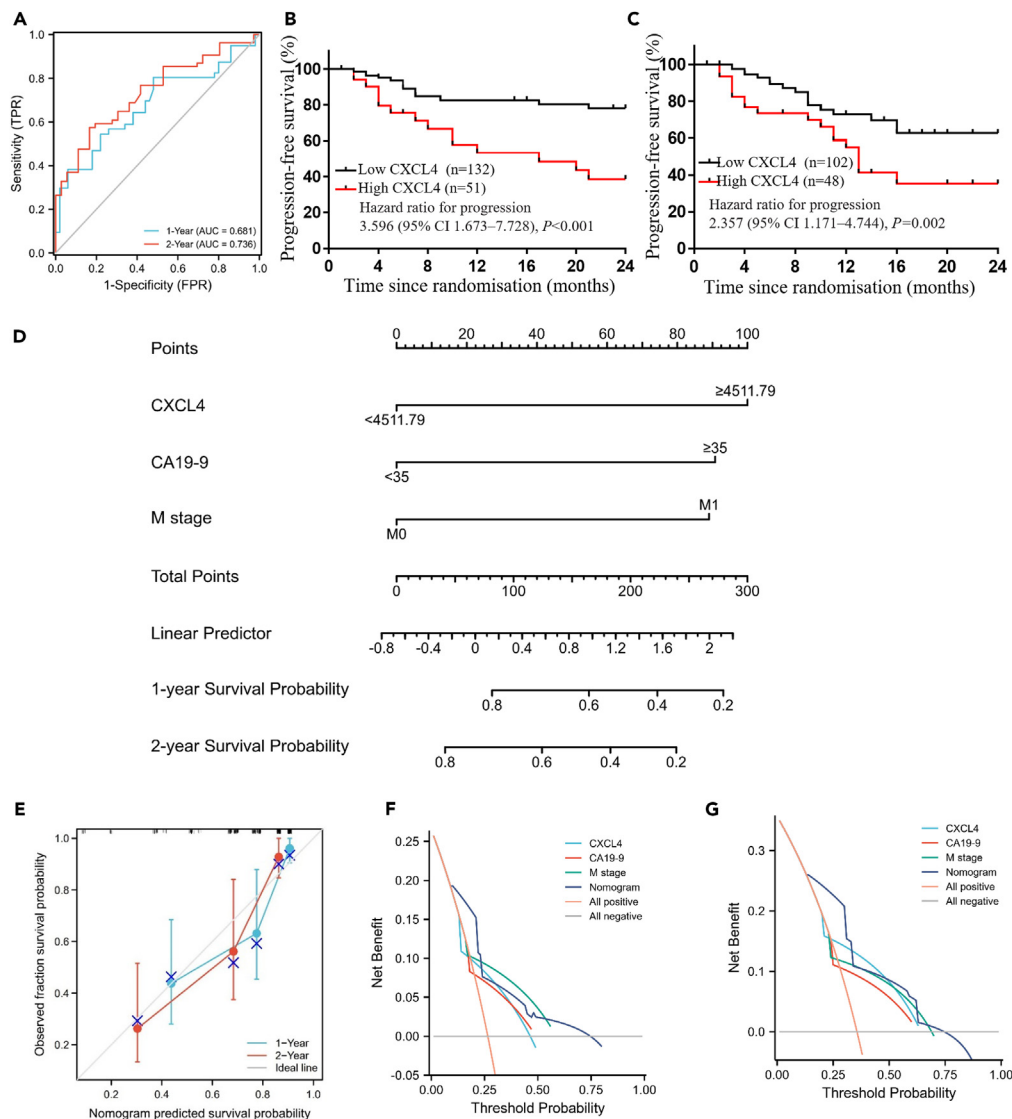
Figure 5. Prognostic outcomes for serum EVs-derived CXCL4 in CRC patients

(A) Time-dependent ROC curves were plotted to calculate the AUCs for 1- and 2- year PFS with serum EVs-derived CXCL4.

(B and C) PFS Kaplan-Meier analysis of CRC patients with low versus high serum EVs-derived CXCL4 in the training cohort (B) and validation cohort (C).

(D) Nomogram model predicting 1- and 2-year PFS in the training cohort.

(E) The calibration curves for predicting 1- and 2-year PFS in the training cohort.

(F and G) Decision curve analysis for 1-year (G) and 2-year (H) PFS predictions in the training cohort. *P* values were calculated using a two-sided log rank test.

detection was laborious. Thus, candidate noninvasive tumor biomarkers with stable results, easy detection, and superior efficacy are required to be explored for clinical application.

With the development of molecular biology, liquid biopsy had become a leading direction in tumor diagnosis due to its noninvasive and dynamic characteristics. Three major types of biomarkers were used in liquid biopsy of tumor patients: circulating tumor cell (CTC), cell-free DNA (cfDNA), and EVs. Since tumor patients contained merely 0–10 CTC cells per milliliter of blood, CTC testing was only recommended for prognostic evaluation of patients with advanced tumors.[25] The DNA fragments released upon the death of normal cells frequently overshadow the cfDNA information of tumor cells.[26] EVs, given their relative stability when encapsulated by vesicular structures, were currently gaining more focus in tumor liquid biopsies.[10] Mature extracellular RNA sequencing methods assisted researchers in characterizing a variety of non-coding RNAs from EVs that could serve as tumor biomarkers. For example, EVs-derived miRNAs (miR-21-5p, miR-141-5p, miR-574-3p) were found to be diagnostic markers for prostate cancer.[27] Moreover, the EVs-derived piRNA, tRNA-GlyGCC-5a had been found to be predictive of disease progression in case of esophageal cancer.[28] Additionally, numerous classical cancer-associated proteins have been

Table 2. Univariate and multivariate Cox hazard analyses of 2-year PFS

| Variables	Univariate analysis		Multivariate analysis	
	HR (95% CI)	p value	HR (95% CI)	p value
Age				
>60 vs. ≤60	0.841 (0.423–1.669)	0.620		
Gender				
Female vs. male	1.325 (0.669–2.622)	0.420		
Differentiation				
Poor vs. moderate/Well	0.705 (0.276–1.803)	0.466		
HER2 expression	0.594 (0.198–1.781)	0.352		
Negative vs. positive				
dMMR/pMMR status	0.482 (0.065–3.592)	0.476		
dMMR vs. pMMR				
CEA (ng/mL)				
≥5 vs. <5	2.112 (1.066–4.183)	0.032		
CA19-9 (ng/mL)				
≥35 vs. <35	3.399 (1.713–6.741)	<0.001	2.478 (1.234–4.976)	0.011
T classification				
T3-T4 vs. T1-T2	4.188 (1.275–13.754)	0.018		
N classification				
N1-N3 vs. N0	3.413 (1.031–11.295)	0.044		
M classification				
M1 vs. M0	4.659 (2.348–9.242)	<0.001	2.435 (1.132–5.239)	0.023
CXCL4 (pg/mL)				
≥4511.79 vs. <4511.79	4.519 (2.218–9.209)	<0.001	2.717 (1.233–5.988)	0.013

discovered in the EVs of cancer patients.[29,30] However, limitations in proteomics impeded progress in identifying candidate tumor biomarker proteins in EVs.

The 4D-DIA proteomics technology, which emerged in 2020, brought proteomics into a new era.[31] Compared with the conventional 3D quantitative protein analysis based on proteolytic digestion, the introduction of the fourth dimension of ion collision cross section has made 4D-DIA proteomics technology the latest quantitative approach, substantially improving the detection depth and quantitative accuracy.[32,33] Through 4D-DIA proteomics techniques, we identified a total of 5,851 peptides and 854 proteins in serum-extracted EVs from 25 CRC patients and 15 HC (Figure 2). Notably, CXCL4 was found to be the most dramatically raised protein in EVs of CRC patients' serum, a result that had never been reported before (Figure S1).

EVs were typically isolated using plasma rather than serum, as plasma was thought to directly reflect blood status in the body. Serum that has undergone procoagulation was thought to potentially affect the release of EVs, making serum-derived EVs often overlooked.[34] Yet, a recent study comparing EVs subpopulations between serum and plasma in the same subjects showed distinct differences between them, with serum EVs exhibiting higher concentrations and carrying more information about physical status.[35] Therefore, our study chose to isolate EVs from serum rather than plasma for screening tumor biomarkers.

CXCL4 was considered a biomarker for systemic sclerosis and respiratory syncytial virus infection.[17,18] Our study observed that both serum EVs-derived CXCL4 and serum-free CXCL4 were markedly enhanced in CRC patients compared to healthy subjects (Figures 3 and 6A–6D). However, serum EVs-derived CXCL4 possessed a superior diagnostic efficacy compared to CEA and CA19-9, which was lacking in serum-free CXCL4 (Figures 4, 6E, and 6F). We hypothesize that this might be attributed to the enrichment of EVs, which amplified CXCL4 signaling secreted by tumor cells and tumor-educated platelets (TEP). The value of TEP in early cancer detection was also highlighted by another research team who used RNA profiling to develop a pan-cancer biomarker panel containing 439 platelet RNAs.[36] Unfortunately, non-cancer diseases, including inflammation, negatively affected the diagnostic specificity of this platelet RNA panel. Still, EVs-derived CXCL4 could distinguish CRC patients from BCP patients, with AUCs of 0.886 and 0.907 in the training and validation cohorts (Figures 4C and 4D). Additionally, the combination of EVs-derived CXCL4, CEA, and CA19-9 showed even better diagnostic efficacy (Figures 4C and S4). Thus, exploring the panel of multiple EVs proteins with the help of machine learning might further optimize the diagnostic effectiveness.

Due to the vulnerability of CRC patients to recurrence, we explored the prognostic role of serum EVs-derived CXCL4. In the training and validation cohorts, serum EV-derived CXCL4 gradually rose as the CRC patient stage progressed (Figures 3D and 3E). Moreover, Kaplan-Meier analysis revealed shorter 2-year PFS for CRC patients with high levels of EVs-derived CXCL4, implying that serum EVs-derived
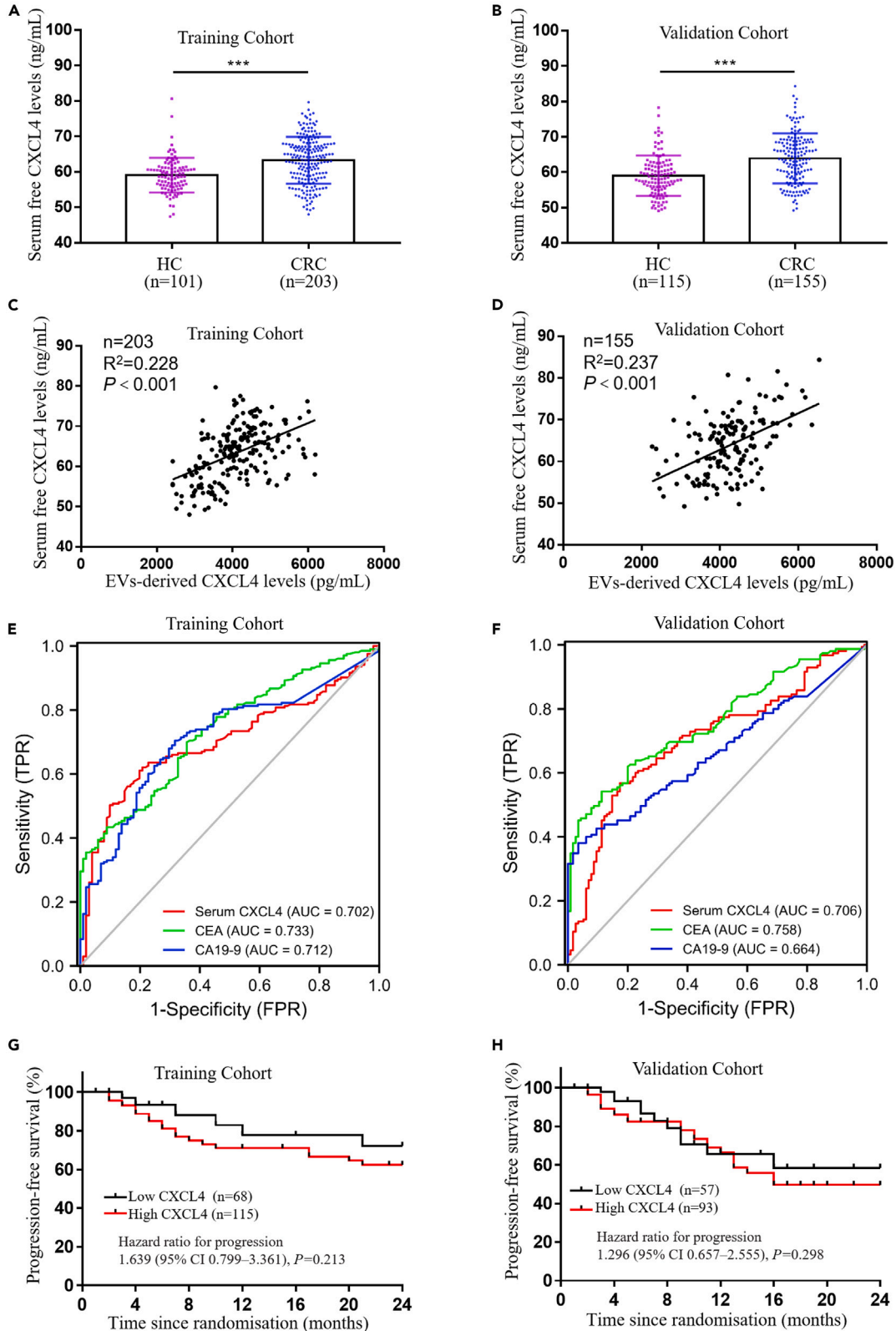
Figure 6. The role of serum-free CXCL4 in the diagnosis and prognosis of CRC
(A) Serum-free CXCL4 levels of CRC patients (n = 203) and HC (n = 101) in the training cohort.
(B) Serum-free CXCL4 levels of CRC patients (n = 155) and HC (n = 115) in the validation cohort.
(C and D) Correlation between serum-free CXCL4 levels and EVs-derived CXCL4 levels of CRC patients in the training cohort (C) and validation cohort (D).
(E and F) ROC curves to identify CRC from HC with serum-free CXCL4 in the training cohort (E) and validation cohort (F).
(G and H) PFS Kaplan-Meier analysis of CRC patients with low versus high serum CXCL4 levels in the training cohort (G) and validation cohort (H).

CXCL4 could serve both as a diagnostic and prognostic indicator (Figures 5B and 5C). Besides, a nomogram prediction model based on Cox regression analysis demonstrated that the combined consideration of CA19-9, M classification, and EVs-derived CXCL4 could further optimize the predictive efficacy (Figures 5D–5G). However, serum-free CXCL4 failed to be a prospective prognostic biomarker for CRC like EVs-derived CXCL4 (Figures 6G and 6H). Additionally, bioinformatics results showed no correlation between CXCL4 transcript levels in CRC tumor tissues and the prognosis of patients.[37] Therefore, these results indicated that the source of CXCL4 likely influenced its role, but further researches were needed to confirm this.

In conclusion, our study demonstrated that serum EVs-derived CXCL4 could serve as a candidate biomarker for the diagnosis and prognosis of CRC with excellent sensitivity and sensitivity, offering a non-invasive manner for large-scale CRC screening. Furthermore, our findings filled the gap between serum EVs-derived proteins and CRC diagnosis, thereby facilitating basic research and clinical applications of EVs in CRC.

Limitations of the study

Despite the promising results of our study, there were several limitations that should be addressed in the future. Firstly, due to time constraints, we collected only 2-year PFS data for predictive analysis. Further follow-up with these patients was needed in order to analyze 5-year overall survival and 5-year PFS. Secondly, the appropriateness of EVs-derived CXCL4 as a specific biomarker for CRC or a pan-cancer biomarker still needed to be validated by a larger number of individuals with different types of tumors. Thirdly, the biological function of EVs-derived CXCL4 has never been reported and deserves further exploration. In fact, it has been suggested that CXCL4 could activate the STAT5/FOXP3 pathway to promote Treg cell production and inhibit CD8^{+} T cell infiltration, mediating a suppressive immune microenvironment to exert pro-tumor effects.[13,14] Moreover, a recent study reported that TEP-secreted EVs protected CTC from natural killer cell-mediated immunosurveillance by participating in the CD94/NKG2A pathway.[38] However, the mechanism by which TEP-secreted EVs regulated CD94 up-regulation in CTC remained unclear, and it would be interesting to explore the potential role of EVs-derived CXCL4 in this process.

STAR★METHODS

Detailed methods are provided in the online version of this paper and include the following:

- KEY RESOURCES TABLE
- RESOURCE AVAILABILITY
  - ○ Lead contact
  - ○ Materials availability
  - ○ Data and code availability
- EXPERIMENTAL MODEL AND STUDY PARTICIPANT DETAILS
  - ○ Clinical sample
  - ○ CRC mouse model
- METHOD DETAILS
  - ○ Serum EVs isolation
  - ○ Transmission electron microscopy (TEM)
  - ○ Nanoparticle tracking analysis (NTA)
  - ○ ELISA detection
  - ○ 4D-DIA quantitative proteomics
- QUANTIFICATION AND STATISTICAL ANALYSIS

SUPPLEMENTAL INFORMATION

Supplemental information can be found online at https://doi.org/10.1016/j.isci.2024.109612.

AUTHOR CONTRIBUTIONS

J.X., J.Z., and H.J. performed the experiments and analyzed the data. S.X. and S.N. collected biological and clinical data. H.Y. and Z.H. conceived and designed this study. D.L. contributed to the reagent preparation. All authors contributed to the article and approved the submitted version.

DECLARATION OF INTERESTS

REFERENCES

1. Cai, J., Sun, L., and Gonzalez, F.J. (2022). Gut microbiota-derived bile acids in intestinal immunity, inflammation, and tumorigenesis. Cell Host Microbe 30, 289–300. https://doi.org/10.1016/j.chom.2022.02.004.

2. Zhang, L., and Shay, J.W. (2017). Multiple Roles of APC and its Therapeutic Implications in Colorectal Cancer. J Natl. Cancer Inst. 109. https://doi.org/10.1093/jnci/djw332.

3. Biller, L.H., and Schrag, D. (2021). Diagnosis and Treatment of Metastatic Colorectal Cancer: A Review. JAMA 325, 669–685. https://doi.org/10.1001/jama.2021.0106.

4. Keum, N., and Giovannucci, E. (2019). Global burden of colorectal cancer: emerging trends, risk factors and prevention strategies. Nat. Rev. Gastroenterol. Hepatol. 16, 713–732. https://doi.org/10.1038/s41575-019-0189-8.

5. Rutter, M.D., Beintaris, I., Valori, R., Chiu, H.M., Corley, D.A., Cuatrecasas, M., Dekker, E., Forsberg, A., Gore-Booth, J., Haug, U., et al. (2018). World Endoscopy Organization Consensus Statements on Post-Colonoscopy and Post-Imaging Colorectal Cancer. Gastroenterology 155, 909–925.e3. https://doi.org/10.1053/j.gastro.2018.05.038.

6. Thomas, D.S., Fourkala, E.O., Apostolidou, S., Gunu, R., Ryan, A., Jacobs, I., Menon, U., Alderton, W., Gentry-Maharaj, A., and Timms, J.F. (2015). Evaluation of serum CEA, CYFRA21-1 and CA125 for the early detection of colorectal cancer using longitudinal preclinical samples. Br. J. Cancer 113, 268–274. https://doi.org/10.1038/bjc.2015.202.

7. Li, C., Zhang, D., Pang, X., Pu, H., Lei, M., Fan, B., Lv, J., You, D., Li, Z., and Zhang, T. (2021). Trajectories of Perioperative Serum Tumor Markers and Colorectal Cancer Outcomes: A Retrospective, Multicenter Longitudinal Cohort Study. EBioMedicine 74, 103706. https://doi.org/10.1016/j.ebiom.2021.103706.

8. Engle, D.D., Tiriac, H., Rivera, K.D., Pommier, A., Whalen, S., Oni, T.E., Alagesan, B., Lee, E.J., Yao, M.A., Lucito, M.S., et al. (2019). The glycan CA19-9 promotes pancreatitis and pancreatic cancer in mice. Science 364, 1156–1162. https://doi.org/10.1126/science.aaw3145.

9. Lai, J.J., Chau, Z.L., Chen, S.Y., Hill, J.J., Korpany, K.V., Liang, N.W., Lin, L.H., Lin, Y.H., Liu, J.K., Liu, Y.C., et al. (2022). Exosome Processing and Characterization Approaches for Research and Technology Development.

10. Yu, D., Li, Y., Wang, M., Gu, J., Xu, W., Cai, H., Fang, X., and Zhang, X. (2022). Exosomes as a new frontier of cancer liquid biopsy. Mol. Cancer 21, 56. https://doi.org/10.1186/s12943-022-01509-9.

11. Min, L., Zhu, S., Chen, L., Liu, X., Wei, R., Zhao, L., Yang, Y., Zhang, Z., Kong, G., Li, P., and Zhang, S. (2019). Evaluation of circulating small extracellular vesicles derived miRNAs as biomarkers of early colon cancer: a comparison with plasma total miRNAs. J. Extracell. Vesicles 8, 1643670. https://doi.org/10.1080/20013078.2019.1643670.

12. Chen, I.H., Xue, L., Hsu, C.C., Paez, J.S., Pan, L., Andaluz, H., Wendt, M.K., Iliuk, A.B., Zhu, J.K., and Tao, W.A. (2017). Phosphoproteins in extracellular vesicles as candidate markers for breast cancer. Proc. Natl. Acad. Sci. USA 114, 3175–3180. https://doi.org/10.1073/pnas.1618088114.

13. Joseph, R., Soundararajan, R., Vasaikar, S., Yang, F., Allton, K.L., Tian, L., den Hollander, P., Isgandarova, S., Haemmerle, M., Mino, B., et al. (2021). CD8(+) T cells inhibit metastasis and CXCL4 regulates its function. Br. J. Cancer 125, 176–189. https://doi.org/10.1038/s41416-021-01338-5.

14. Xu, T., Zhao, J., Wang, X., Meng, Y., Zhao, Z., Bao, R., Deng, X., Bian, J., and Yang, T. (2020). CXCL4 promoted the production of CD4(+) CD25(+)FOXP3(+)treg cells in mouse sepsis model through regulating STAT5/FOXP3 pathway. Autoimmunity 53, 289–296. https://doi.org/10.1080/08916934.2020.1777283.

15. Quemener, C., Baud, J., Boyé, K., Dubrac, A., Billottet, C., Soulet, F., Darlot, F., Dumartin, L., Sire, M., Grepin, R., et al. (2016). Dual Roles for CXCL4 Chemokines and CXCR3 in Angiogenesis and Invasion of Pancreatic Cancer. Cancer Res. 76, 6507–6519. https://doi.org/10.1158/0008-5472.CAN-15-2864.

16. Reynders, N., Abboud, D., Baragli, A., Noman, M.Z., Rogister, B., Niclou, S.P., Heveker, N., Janji, B., Hanson, J., Szpakowska, M., and Chevigné, A. (2019). The Distinct Roles of CXCR3 Variants and Their Ligands in the Tumor Microenvironment. Cells 8, 613. https://doi.org/10.3390/cells8060613.

17. van Bon, L., Affandi, A.J., Broen, J., Christmann, R.B., Marijnissen, R.J., Stawski, L., Farina, G.A., Stifano, G., Mathes, A.L., Cossu, M., et al. (2014). Proteome-wide analysis and CXCL4 as a biomarker in systemic sclerosis. N. Engl. J. Med. 370,

Adv. Sci. 9, e2103222. https://doi.org/10.1002/advs.202103222.

433–443. https://doi.org/10.1056/NEJMoa1114576.

18. Han, Z., Rao, J., Xie, Z., Wang, C., Xu, B., Qian, S., Wang, Y., Zhu, J., Yang, B., Xu, F., et al. (2020). Chemokine (C-X-C Motif) Ligand 4 Is a Restrictor of Respiratory Syncytial Virus Infection and an Indicator of Clinical Severity. Am. J. Respir. Crit. Care Med. 202, 717–729. https://doi.org/10.1164/rccm.201908-1567OC.

19. Affandi, A.J., Carvalheiro, T., Ottria, A., de Haan, J.J., Brans, M.A.D., Brandt, M.M., Tieland, R.G., Lopes, A.P., Fernández, B.M., Bekker, C.P.J., et al. (2022). CXCL4 drives fibrosis by promoting several key cellular and molecular processes. Cell Rep. 38, 110189. https://doi.org/10.1016/j.celrep.2021.110189.

20. Gleitz, H.F.E., Dugourd, A.J.F., Leimkühler, N.B., Snoeren, I.A.M., Fuchs, S.N.R., Menzel, S., Ziegler, S., Kröger, N., Triviai, I., Büsche, G., et al. (2020). Increased CXCL4 expression in hematopoietic cells links inflammation and progression of bone marrow fibrosis in MPN. Blood 136, 2051–2064. https://doi.org/10.1182/blood.2019004095.

21. Wang, Z., Wang, Z., Li, G., Wu, H., Sun, K., Chen, J., Feng, Y., Chen, C., Cai, S., Xu, J., and He, Y. (2017). CXCL1 from tumor-associated lymphatic endothelial cells drives gastric cancer cell into lymphatic system via activating integrin beta1/FAK/AKT signaling. Cancer Lett. 385, 28–38. https://doi.org/10.1016/j.canlet.2016.10.043.

22. Zhou, Z., Xia, G., Xiang, Z., Liu, M., Wei, Z., Yan, J., Chen, W., Zhu, J., Awasthi, N., Sun, X., et al. (2019). A C-X-C Chemokine Receptor Type 2-Dominated Cross-talk between Tumor Cells and Macrophages Drives Gastric Cancer Metastasis. Clin. Cancer Res. 25, 3317–3328. https://doi.org/10.1158/1078-0432.CCR-18-3567.

23. Yin, H., Huang, Z., Niu, S., Ming, L., Jiang, H., Gu, L., Huang, W., Xie, J., He, Y., and Zhang, C. (2022). 5-Methylcytosine (m(5)C) modification in peripheral blood immune cells is a novel non-invasive biomarker for colorectal cancer diagnosis. Front. Immunol. 13, 967921. https://doi.org/10.3389/fimmu.2022.967921.

24. Xie, H., Huang, Z., Jiang, P., Wu, R., Jiang, H., Luo, C., Hong, H., and Yin, H. (2021). Elevated N6-Methyladenosine RNA Levels in Peripheral Blood Immune Cells: A Novel Predictive Biomarker and Therapeutic Target for Colorectal Cancer. Front. Immunol. 12,

760747. https://doi.org/10.3389/fimmu.2021.760747.

25. Thanh Huong, P., Gurshaney, S., Thanh Binh, N., Gia Pham, A., Hoang Nguyen, H., Thanh Nguyen, X., Pham-The, H., Tran, P.T., Truong Vu, K., Xuan Duong, N., et al. (2020). Emerging Role of Circulating Tumor Cells in Gastric Cancer. Cancers 12, 695. https://doi.org/10.3390/cancers12030695.

26. Ren, J., Lu, P., Zhou, X., Liao, Y., Liu, X., Li, J., Wang, W., Wang, J., Wen, L., Fu, W., and Tang, F. (2022). Genome-Scale Methylation Analysis of Circulating Cell-Free DNA in Gastric Cancer Patients. Clin. Chem. 68, 354–364. https://doi.org/10.1093/clinchem/hvab204.

27. Ramirez-Garrastacho, M., Berge, V., Linē, A., and Llorente, A. (2022). Potential of miRNAs in urinary extracellular vesicles for management of active surveillance in prostate cancer patients. Br. J. Cancer 126, 492–501. https://doi.org/10.1038/s41416-021-01598-1.

28. Li, K., Lin, Y., Luo, Y., Xiong, X., Wang, L., Durante, K., Li, J., Zhou, F., Guo, Y., Chen, S., et al. (2022). A signature of saliva-derived exosomal small RNAs as predicting biomarker for esophageal carcinoma: a multicenter prospective study. Mol. Cancer 21, 21. https://doi.org/10.1186/s12943-022-01499-8.

29. Sun, N., Zhang, C., Lee, Y.T., Tran, B.V., Wang, J., Kim, H., Lee, J., Zhang, R.Y., Wang, J.J., Hu, J., et al. (2023). HCC EV ECG score: An extracellular vesicle-based protein assay for detection of early-stage hepatocellular

carcinoma. Hepatology 77, 774–788. https://doi.org/10.1002/hep.32692.

30. Zhang, Z., Liu, X., Yang, X., Jiang, Y., Li, A., Cong, J., Li, Y., Xie, Q., Xu, C., and Liu, D. (2023). Identification of faecal extracellular vesicles as novel biomarkers for the non-invasive diagnosis and prognosis of colorectal cancer. J. Extracell. Vesicles 12, e12300. https://doi.org/10.1002/jev2.12300.

31. Meier, F., Brunner, A.D., Frank, M., Ha, A., Bludau, I., Voytik, E., Kaspar-Schoenefeld, S., Lubeck, M., Raether, O., Bache, N., et al. (2020). diaPASEF: parallel accumulation-serial fragmentation combined with data-independent acquisition. Nat. Methods 17, 1229–1236. https://doi.org/10.1038/s41592-020-00998-0.

32. Lin, H., Zhang, W., Xu, Y., You, Z., Zheng, M., Liu, Z., and Li, C. (2022). 4D label-free quantitative proteomics analysis to screen potential drug targets of Jiangu Granules treatment for postmenopausal osteoporotic rats. Front. Pharmacol. 13, 1052922. https://doi.org/10.3389/fphar.2022.1052922.

33. Yang, X., Li, X., Zhu, Y., Gao, Y., and Xu, L. (2022). Paeoniflorin Upregulates Mitochondrial Thioredoxin of Schwann Cells to Improve Diabetic Peripheral Neuropathy Indicated by 4D Label-Free Quantitative Proteomics. Oxid. Med. Cell. Longev. 2022, 4775645. https://doi.org/10.1155/2022/4775645.

34. Karimi, N., Cvjetkovic, A., Jang, S.C., Crescitelli, R., Hosseinpour Feizi, M.A., Nieuwland, R., Lötvall, J., and Lässer, C. (2018). Detailed analysis of the plasma

extracellular vesicle proteome after separation from lipoproteins. Cell. Mol. Life Sci. 75, 2873–2886. https://doi.org/10.1007/s00018-018-2773-4.

35. Karimi, N., Dalirfardouei, R., Dias, T., Lötvall, J., and Lässer, C. (2022). Tetraspanins distinguish separate extracellular vesicle subpopulations in human serum and plasma - Contributions of platelet extracellular vesicles in plasma samples. J. Extracell. Vesicles 11, e12213. https://doi.org/10.1002/jev2.12213.

36. In 't Veld, S., Arkani, M., Post, E., Antunes-Ferreira, M., D'Ambrosi, S., Vessies, D.C.L., Vermunt, L., Vancura, A., Muller, M., Niemeijer, A.N., et al. (2022). Detection and localization of early- and late-stage cancers using platelet RNA. Cancer Cell 40, 999–1009.e1006. https://doi.org/10.1016/j.ccell.2022.08.006.

37. Yu, L., Yang, X., Xu, C., Sun, J., Fang, Z., Pan, H., and Han, W. (2020). Comprehensive analysis of the expression and prognostic value of CXC chemokines in colorectal cancer. Int Immunopharmacol. 89, 107077. https://doi.org/10.1016/j.intimp.2020.107077.

38. Liu, X., Song, J., Zhang, H., Liu, X., Zuo, F., Zhao, Y., Zhao, Y., Yin, X., Guo, X., Wu, X., et al. (2023). Immune checkpoint HLA-E:CD94-NKG2A mediates evasion of circulating tumor cells from NK cell surveillance. Cancer Cell 41, 272–287.e9. https://doi.org/10.1016/j.ccell.2023.01.001.

STAR★METHODS

KEY RESOURCES TABLE

REAGENT or RESOURCE	SOURCE	IDENTIFIER
Biological samples		
Serum samples from patients	The Seventh Affiliated Hospital of Sun Yat-Sen University	This paper
Serum samples from patients	Sun Yat-sen University Cancer Center	This paper
Critical commercial assays		
Human CXCL4 ELISA Kit	Neobioscience	EHC135.96
Mouse CXCL4 ELISA Kit	Neobioscience	EMC015.96
Deposited data		
Mass spectrometry data	iProX database	IPX0008187000
Experimental models: Cell lines		
MC38	Procell Life Science&Technology	RRID:CVCL_B288
Experimental models: Organisms/strains		
C57BL/6	Charles River	RRID:MGI:2159769
Apc-L850X	Shanghai Model Organisms Center	RRID:IMSR_NM-KI-200001
Software and algorithms		
R (version 4.2.1)	R Project	https://www.r-project.org
SPSS 26.0	IBM	RRID:SCR_002865
GraphPad Prism	GraphPad Software	RRID:SCR_002798

RESOURCE AVAILABILITY

Lead contact

For additional details and inquiries regarding resources and reagents, please contact the primary point of contact, Haofan Yin (e-mail: yinhf@mail2.sysu.edu.cn).

Materials availability

This study did not generate new unique reagents.

Data and code availability

- The mass spectrometry proteomics data have been deposited to the ProteomeXchange Consortium with the dataset identifier IPX0008187000.
- This paper does not report original code.
- Any additional information required to reanalyze the data reported in this paper is available from the lead contact upon request.

EXPERIMENTAL MODEL AND STUDY PARTICIPANT DETAILS

Clinical sample

The study population was all Han Chinese. The discovery cohort consisted of 15 healthy controls (HCs, male: 7, female: 8) and 25 CRC (male: 12, female: 13) patients before treatment. Between May 2022 and June 2022, the serum of HC and CRC were collected from Sun Yat-sen University Cancer Center.

The training cohort consisted of 101 HC (male: 57, female: 44), 203 CRC (male: 116, female: 87) patients before treatment, and 47 benign colorectal polyp (BCP, male: 26, female: 21) patients. Between August 2020 and October 2022, the serum of these individuals were all collected from Sun Yat-sen University Cancer Center.

The validation cohort consisted of 115 HC (male: 60, female: 55), 194 CRC patients (male: 113, female: 81) and 55 BCP (male: 38, female: 55) patients. Between September 2020 and December 2022, the serum of these individuals were all collected from The Seventh Affiliated Hospital of Sun Yat-Sen University. The CRC group included 155 cases of CRC patients before treatment and 39 cases of CRC patients after treatment.

None of the enrolled HC suffered from intestinal diseases, any inflammatory diseases or other diseases. All CRC were diagnosed on the basis of histopathological examination and serum samples were collected at diagnosis prior to tumor resection or chemoradiotherapy, except for 39 post-treatment CRC patients in the validation cohort. BCP was diagnosed on the basis of standard endoscopic, histologic, and radiographic criteria. Informed consent was obtained for all individuals. Ethics approval was obtained from the Ethics Committee of The Seventh Affiliated Hospital of Sun Yat-Sen University (KY-2020-039-01) and Sun Yat-sen University Cancer Center (B2022-475-01) and. The clinical and biological characteristics of the individuals were described in Tables S1 and S2.

CRC mouse model

All animals were kept in Shenzhen TopBiotech Co., Ltd and were male. Apc-L850X mice, a model of spontaneous CRC, were purchased from Shanghai Model Organisms Center, Inc, were sacrificed for collection serum at 12 weeks old. Additionally, C57BL/6 mice were purchased from Charles River Co. Ltd (Beijing, China). 1×10^6 MC38 cells were injected into the inguinal folds of C57BL/6 to construct the MC38 Syngeneic CRC mouse model. These mice were sacrificed for collection serum at 28 days after injection. All procedures related to animal feeding, treatment, and welfare were conducted following with the Institutional Animal Care and Use Committee of Shenzhen TopBiotech Co., Ltd.

METHOD DETAILS

Serum EVs isolation

The fresh blood collected from the individuals were added to the vacuum blood tube, and centrifuged at 4000 g for 20 min. Then, 1 mL supernatant serum was stored at $-80°C$. After the required number of samples were collected, they were uniformly thawed and used for EVs extraction. After the frozen serum was thawed on ice, the supernatant was collected by centrifugation at 10,000 g for 20 min. Dilute the supernatant with 4 mL cold PBS and add it to the 0.22 μm filter. After the filtered supernatant was centrifuged at 120,000 g for 90 min, the supernatant was aspirated, leaving the pellet at the bottom of the tube. The pellet was then resuspended in 4 mL PBS and centrifuged at 120,000 g for 90 min again. After carefully aspirating the supernatant, the remaining precipitate was the high purity EVs. The isolated EVs samples were resuspended in 100 μL PBS and stored at $-80°C$.

Transmission electron microscopy (TEM)

Dropped 10 μL of EVs suspension onto the copper grid with carbon film for 3 min, and use filter paper to absorb the excess liquid. Then, dropped 2% phosphotungstic acid on the copper grid to stain for 2 min, and use filter paper to absorb excess liquid. Finally, the cuprum grids were photographed under TEM HT7800 (Hitachi, Tokyo, Japan).

Nanoparticle tracking analysis (NTA)

The EVs samples were diluted with PBS (dilution 1:1000) and subsequently detected directly using a nanoparticle tracking analyzer ZetaVIEW S/N 21–734 (Particle Metrix, Munich, Germany).

ELISA detection

ELISA kits were used to detect the level of CXCL4 protein derived from human serum EVs (Neobioscience, EHC135.96) and the level of CXCL4 protein derived from mouse serum EVs (Neobioscience, EMC015.96), respectively. 10 μL EV sample were placed on ice using 90 μL RIPA lysate for 60 min and then the samples were diluted with 200 μL PBS. Next, 100 μL diluted samples were added to the 96-well plate for ELISA detection according manufacturer's protocol. Finally, using synergyH1 multi-modelreaders (BioTek, Vermont, USA) to measure the absorbance at 450 nm.

4D-DIA quantitative proteomics

4D-DIA quantitative proteomics were performed by Shanghai Genechem Co., Ltd. 40 serum samples in the discovery cohort were digested into peptides by FASP. The peptide samples were diluted to 10 ng/μL with 0.1% formic acid and supplemented with iRT peptide mixture. Each sample was loaded with 200 ng of peptides and desalted using Evotips. Separation was performed using the nanoflow Evosep system, coupled to a timsTOF Pro mass spectrometer equipped with a CaptiveSpray ion source. Buffer A consisted of 0.1% aqueous formic acid, while buffer B comprised 0.1% formic acid in acetonitrile. Chromatographic separation was conducted using the 30SPD method provided by Evosep One. Following chromatographic separation on Evosep One, samples underwent mass spectrometric analysis using the PASEF mode of the timsTOF Pro Mass Spectrometer (Bruker, Bremen, Germany). Ionization was conducted in positive ion mode with a mass range of 100–1700 m/z. The 1/K0 ion mobility range was set to 0.6–1.6 V·s/cm^2, with an ion accumulation/release time of 100 ms and a 100% ion utilization rate. The capillary voltage was set to 1500 V, and the drying gas flow rate was 3 L/min with a drying temperature of 180°C. PASEF settings included 10 MS/MS scans (total cycle time: 1.16 s), a charge range of 0–5, dynamic exclusion time of 0.4 min, ion target intensity of 10,000, ion intensity threshold of 2500, and collision-induced dissociation energy of 20–59 eV. Raw Data of DIA were processed and analyzed by Spectronaut (Biognosys AG, Switzerland) with default settings, Retention time prediction type was set to dynamic iRT. Spectronaut will determine the ideal extraction window dynamically depending on iRT calibration and gradient stability.

QUANTIFICATION AND STATISTICAL ANALYSIS

Statistical analyses were performed with the IBM SPSS Statistics 26.0 and R version 4.2.1. The data variability, which was presented as the SD (mean $\pm$ SD), was analyzed via unpaired Student's t test between two groups for normally distributed data. Otherwise, the data was analyzed via nonparametric Mann–Whitney test. Receiver operating characteristics (ROC) curves were plotted to assess area under the curve (AUC) (95% confidence interval (CI)). We considered the value with the maximization of the Yuden index as the cut-off value. Kaplan-Meier analysis was used to evaluate progression-free survival (PFS) using a two-sided log rank test. The univariate and multivariate analyses were executed using the Cox proportional hazards model and were shown as hazard ratios (HR). All variables in the multivariable model were enrolled to construct a prognostic nomogram model. Calibration of the nomogram for 1- and 2-year PFS were presented by comparing the observed survival with predicted survival. $p < 0.05$ was defined statistical significance.